

UNIVERSITY OF LEIPZIG

ADVANCED LABS

Lab report

RF Technique and Electron-Paramagnetic Resonance (EPR)

Jamal Ghaith

Anas Roumieh

Conducted on: 11.06.2024

Contents

1	Introduction	1
1.1	EPR	1
1.2	Zeeman effect	1
1.3	Resonance condition	1
1.4	EPR spectrum	2
1.5	RF techniques	2
1.5.1	Frequency modulation	2
1.5.2	Frequency mixing	3
1.6	Materials	3
1.6.1	DPPH	3
1.6.2	Ultramarine	3
1.7	Experimental Setup	4
2	Analysis	7
2.1	Task 1: <i>Frequency mixing and modulation</i>	7
2.2	Task 2: <i>Receiving and analyzing signals in the VLF range from 10 kHz to 150 kHz</i>	7
2.3	Task 4: <i>Determination of the resonance frequency and recording of the dispersion curves of different DPPH samples</i>	8
2.4	Task 5: <i>Determination of the resonance frequency and recording of the dispersion curves of different Ultramarine samples</i>	9
2.5	Task 6: <i>Measurement of the DPPH sample 10 µg with a calibrated LNB as observation system</i>	11
3	Conclusion	12
	Bibliography	13

1 Introduction

1.1 EPR

Electron paramagnetic resonance (EPR) or electron spin resonance is a spectroscopy method used to study molecules or atoms which have unpaired electrons. A paramagnetic sample is placed in a magnetic field and irradiated with microwaves which interact with the spins of the unpaired electrons.

1.2 Zeeman effect

When an external magnetic field is applied to a paramagnetic substance, the spins of the unpaired electrons can align either parallel or anti-parallel to the direction of the magnetic field, resulting in spin states of $m_s = \pm \frac{1}{2}$. These alignments correspond to different energy levels, thus lifting the degeneracy of the electron spin states. The energy difference between those levels is:

$$\Delta E = g\mu_B B \quad (1)$$

Here, B is the applied magnetic field, μ_B is the Bohr magneton and g is the Lande g-factor which gives the relation between a magnetic moment and the angular momentum of an electron system. For a free electron $g = 2.0023$. The splitting of the energy levels due to the interaction between the magnetic field and the magnetic moment of the electron is known as the Zeeman effect.

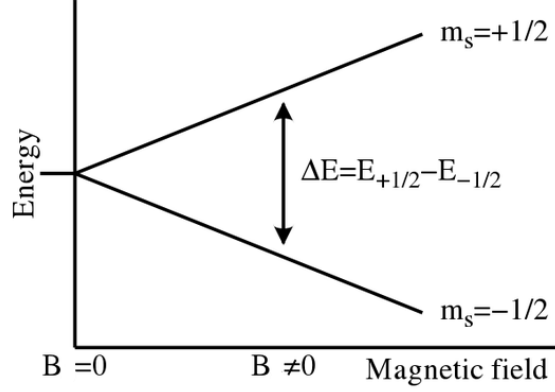


Figure 1: Zeeman splitting [6]

1.3 Resonance condition

An unpaired electron can change its spin by absorbing or emitting a photon with energy $h\nu$, in accordance with the resonance condition $h\nu = \Delta E$. This gives rise to the fundamental equation of EPR spectroscopy:

$$h\nu_0 = g\mu_B B_0 \quad (2)$$

1.4 EPR spectrum

The vast majority of EPR measurements are conducted using microwaves in the 9000 MHz to 10 000 MHz range (9 GHz to 10 GHz), with magnetic fields approximately around 0.35 T. EPR spectra can be generated by either varying the photon frequency incident on a sample while keeping the magnetic field constant or by varying the magnetic field while keeping the frequency constant. In practice, it is usually the frequency that is kept fixed. By increasing the external magnetic field, the energy gap between the $m_s = +\frac{1}{2}$ and $m_s = -\frac{1}{2}$ states widens until it equals the energy of the microwaves. Because more electrons are generally found in the lower energy state due to the Maxwell–Boltzmann distribution, there is an overall absorption of energy. This absorption is what is detected and transformed into a spectrum. The EPR spectrum is the derivative of the absorption peak (see Figure 2).

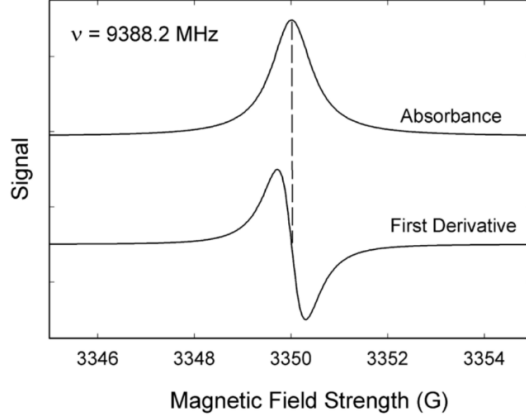


Figure 2: EPR Spectrum [6]

1.5 RF techniques

1.5.1 Frequency modulation

Frequency modulation is a radio frequency technique that involves altering a periodic waveform using another waveform. Frequency modulation allows the frequency of a specific RF carrier signal to be altered based on another signal, the modulation signal. This technique can be beneficial for distinguishing an RF signal from other RF signals in the spectrum. It is a very important method for radio communication.

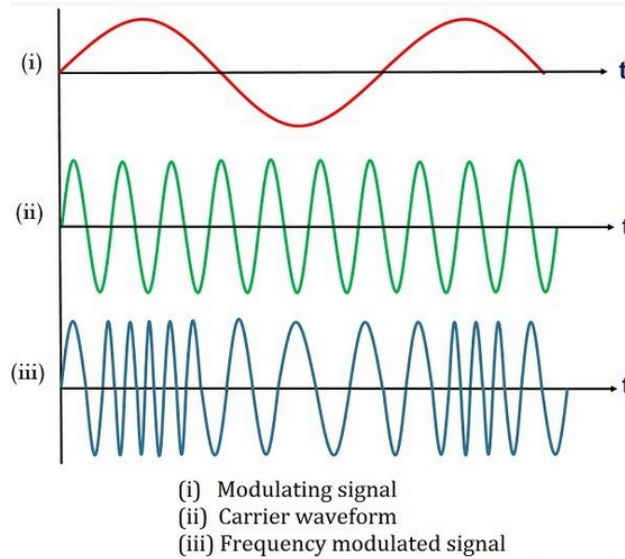


Figure 3: Frequency modulation [3]

1.5.2 Frequency mixing

Frequency mixing is a process where a signal with a new frequency is created from two other signals. In its most common use, a mixer combines two signals and generates new signals at the sum and difference of the original frequencies. In a practical frequency mixer, additional frequency components may also be produced. The signals are multiplied together, resulting in the complicated shape as shown in 4.

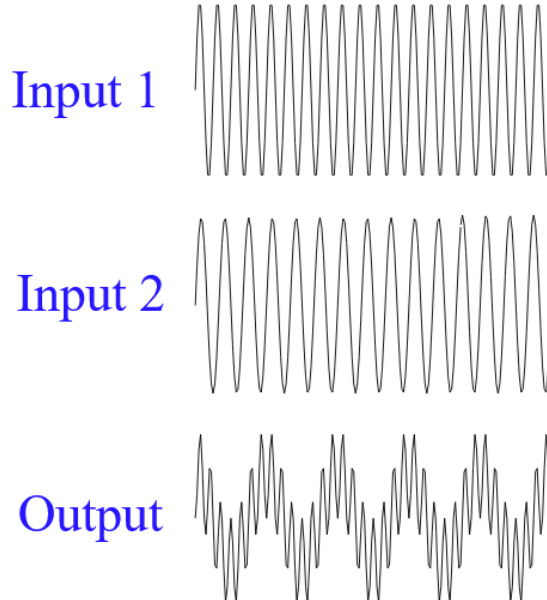


Figure 4: Frequency mixing [2]

1.6 Materials

The materials mainly used in EPR measurements are:

- free radicals in solid state materials, liquids or gases
- paramagnetic transition metal ions

DPPH and Ultramarine in different concentrations were used as samples.

1.6.1 DPPH

Diphenyl-Picryl-Hydrazyl (DPPH) is a common used material for EPR measurements. It is a crystalline powder which has a dark color and has an unpaired electron. Its g-factor is $g = 2.0036$, which is close to the g-factor of an electron.

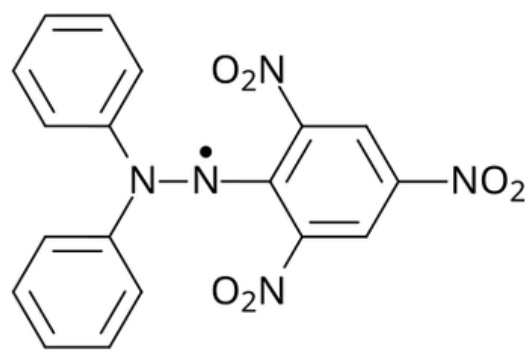


Figure 5: DPPH [5]

1.6.2 Ultramarine

Ultramarine (UM) is another widely used substance for EPR measurements due to its strong paramagnetic characteristics. Its g-factor is $g = 2.0290$ and therefore differs strongly from the g-factor of an electron. Its chemical formula is $\text{Na}_{8-10}\text{Al}_{16}\text{Si}_6\text{O}_{24}\text{S}_{2-4}$

1.7 Experimental Setup

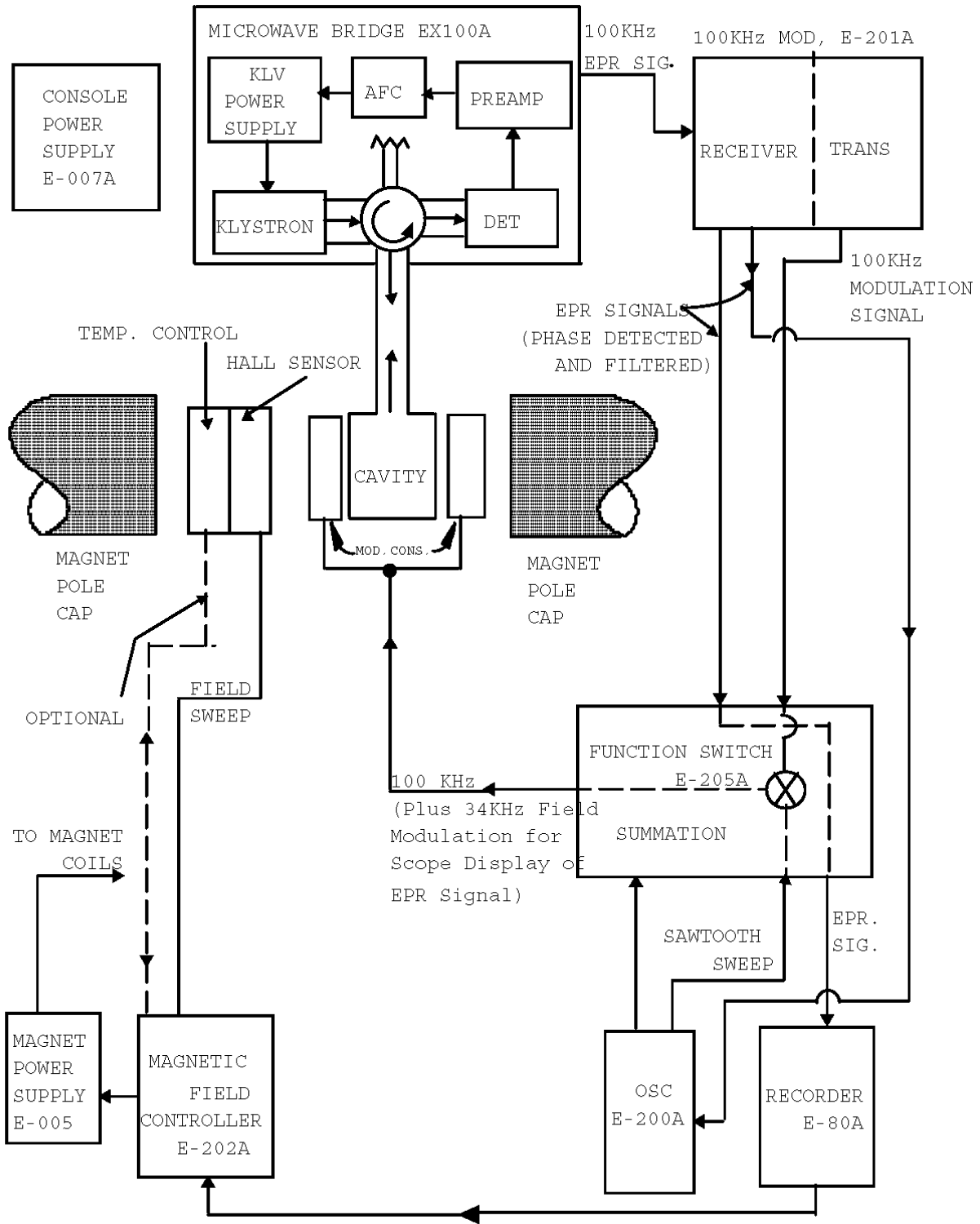


Figure 6: Experimental setup for the EPR experiment. [8]

Figure 6 shows the experiment setup of an EPR spectrometer. It mainly consists of: the microwave bridge and the receiving system with the magnets.

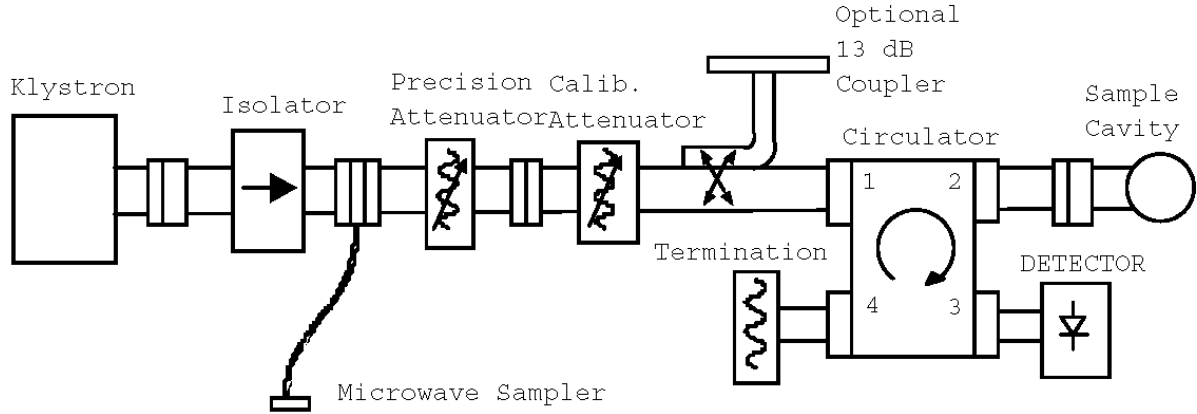


Figure 7: Microwave cavity. [8]

Figure 7 shows the microwave cavity which is used to generate the microwaves, and detection of the EPR signal. It consists of a klystron, an attenuator, a circulator, and a sample cavity resonator.

- Klystron: Generates microwaves in the X-Band frequency range (8-12 GHz).
- Attenuator: Used to adjust the power of the microwaves.
- Circulator: Directs the microwaves to the sample cavity, and reflects energy from the cavity to the detector.
- Sample Cavity: Acts like a tuned circuit with very high Q-factor ($Q = \frac{\omega \cdot \text{Energy stored}}{\text{Power dissipated in cavity}}$). When this sample cavity is in resonance with the microwaves, the impedance of the cavity changes causing the signal to be reflected back to the crystal detector.

As aforementioned, the microwave frequency remains constant while the external magnetic field is swept through the resonance condition. To amplify the EPR signal, a high-frequency modulated magnetic field is added to the slowly swept magnetic field. This approach also reduces noise and improves spectral resolution. The enhancements occur because the sample reacts to the modulated magnetic field, altering the signal's amplitude. This change corresponds to the difference in absorbed energy within the resonator cavity. Noise is eliminated from the measured signal since the signal's phase and frequency are known.

The high-frequency modulation is introduced using small coils positioned on each side of the cavity walls along the axis of the static field. Typically, a frequency of 100 kHz is used.

The modulation amplitude should be smaller than the resonance line width. This ensures that the detected 100 kHz signal is proportional to the slope of the absorption curve. Consequently, at resonance (corresponding to the zero curve), the 100 kHz component at the detector is zero. Similarly, the maximum slope occurs at the inflection point where the output signal is also at its maximum. The polarity of the output signal from the phase-sensitive detector is determined by the slope's sign. Therefore, with small modulation amplitudes, the output signal approximates the first derivative of the absorption signal. However, using higher modulation amplitudes closer to the line width value results in distorted line shapes.

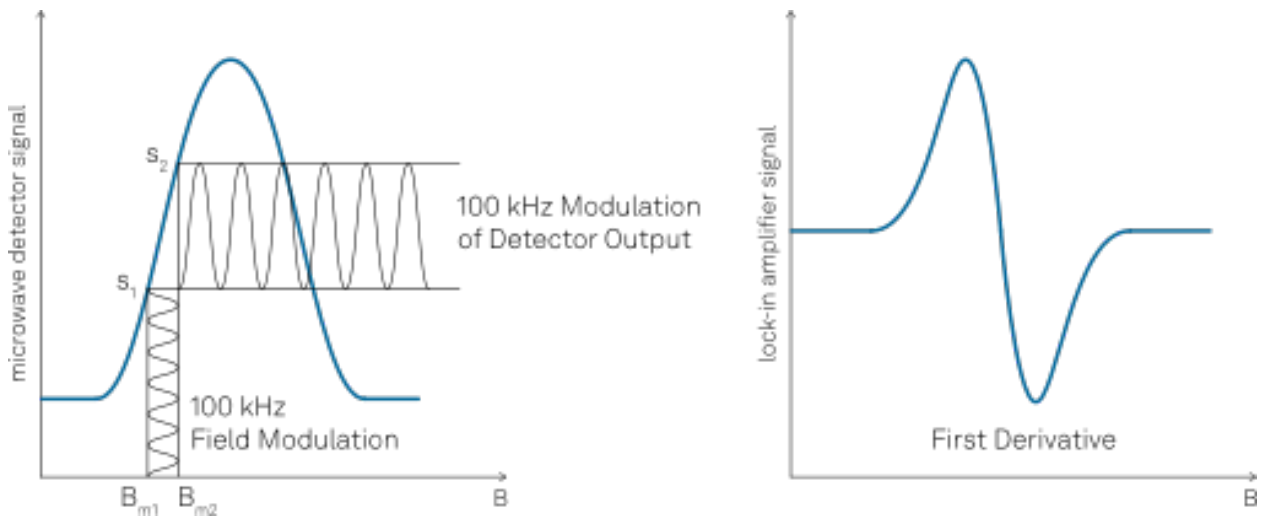


Figure 8: Magnetic field modulation. [4]

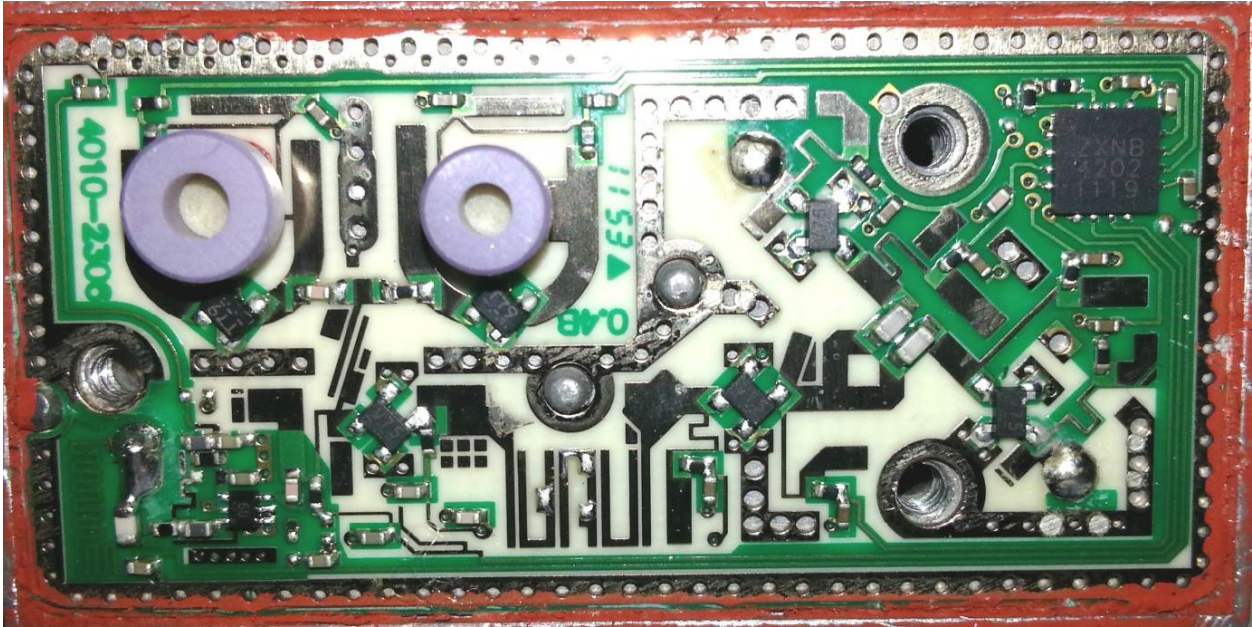


Figure 9: Low-noise block. [7]

The low-noise block (LNB), also known as a modified low-noise block down converter, is used for EPR measurements on the DPPH and ultramarine samples. An LNB typically combines a frequency mixer, local oscillators, and a down converter. It also includes a low-noise amplifier that boosts a low-power signal while maintaining nearly the same signal-to-noise ratio.

Figure 9 shows the LNB used, where the two violet ring cylinders represent the local oscillators (LOs). Each LO generates a specific frequency: one at 9.75 GHz and the other at 10.6 GHz. These frequencies are mixed by a mixer, producing both the sum and difference frequencies of the two LOs, with only the difference frequency being considered. This resulting frequency is then processed through a down converter, shifting it to around 800 MHz at the output. The samples are exposed to the dielectric resonator with the 10.6 GHz frequency, depicted as the smaller violet ring cylinder on the right. This setup allows for the measurement of dispersion signals.

2 Analysis

2.1 Task 1: Frequency mixing and modulation

Here we were tasked with observing the signals that would result from a frequency mixer with $f_1 = 10$ MHz and f_2 varying from 200 to 1000 kHz. This is what we saw on the oscilloscope:

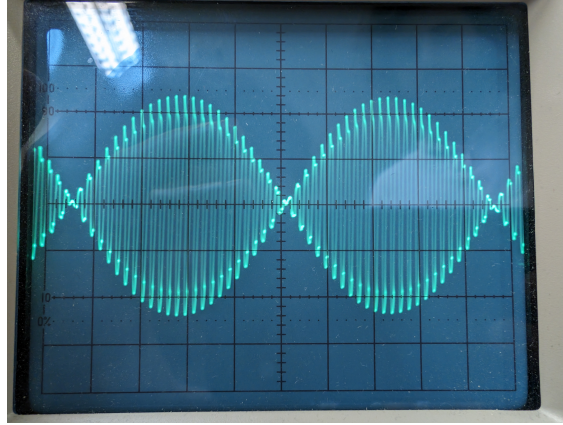


Figure 10: Oscilloscope output with $f_1 = 10$ MHz and $f_2 = 200$ kHz.

This is what we saw on the HDSDR software:

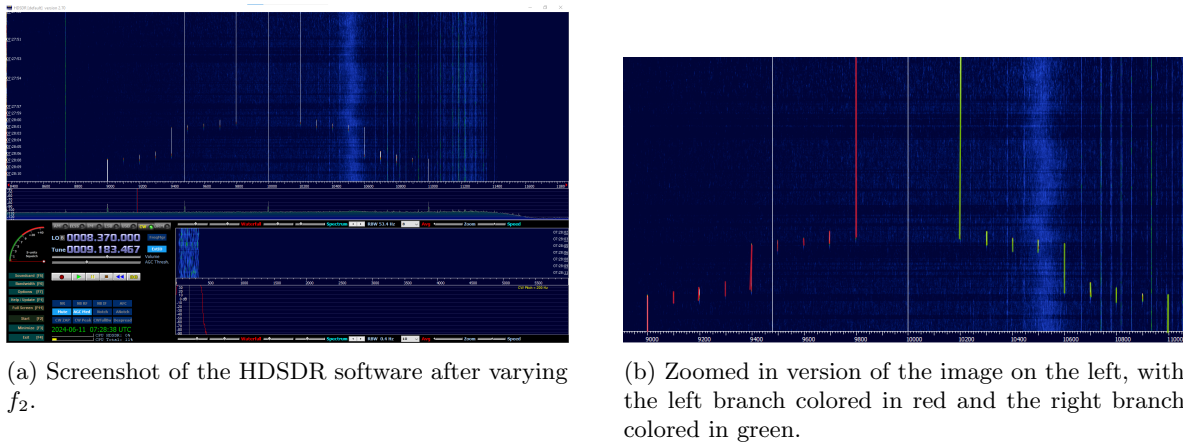


Figure 11: Frequency mixing

Figure 11b shows the two main branches of the signal. The right one, in green, is the result of the addition of the two frequencies ($f_1 + f_2$), while the left one, in red, is the result of their subtraction ($f_1 - f_2$). We varied in steps of 100 kHz which can clearly be seen in the image. The left one ends at 9 MHz and the right one at 11 MHz; corresponding to the frequencies 10 ± 1 MHz.

The two other lines that are observed are at 10 MHz and 9.458 MHz. The 10 MHz line is there for obvious reasons, but the other is odd, maybe due to some interference or noise.

2.2 Task 2: Receiving and analyzing signals in the VLF range from 10 kHz to 150 kHz

Here we were tasked with observing signals what would arise from varying the channels on a simple radio transmitter (walkie-talkie).

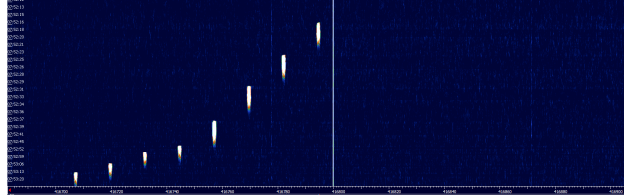


Figure 12: HDSDR screenshot with the walkie-talkie on different channels.

As we went from channel 1 to channel 8, the frequency decreased from ≈ 416795 KHz down to ≈ 416708 in increments of ≈ 12 kHz.

2.3 Task 4: Determination of the resonance frequency and recording of the dispersion curves of different DPPH samples

We were provided with two DPPH of different weights; 1 μg and 10 μg . We were tasked with recording the dispersion curves and then finding the resonance frequency, which was done by taking screenshots of the software and converting it to points using WebPlotDigitizer. [1]

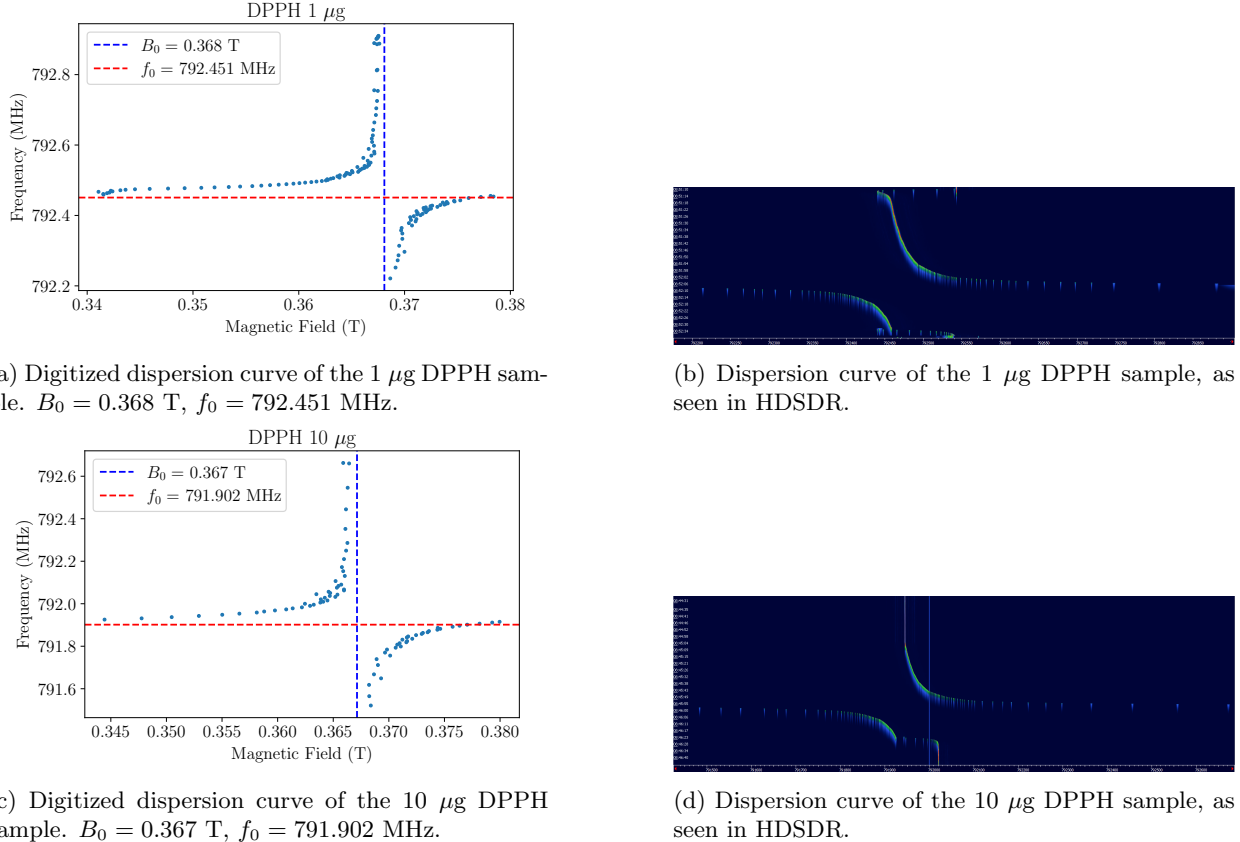


Figure 13

using the data from the digitized dispersion curves, we can calculate the g-factor of the DPPH samples by solving for g in equation 2, such that:

$$g = \frac{h\nu_0}{\mu_B B_0}$$

The following table shows the calculated g-factors for the two samples:

DPPH g-factor	Theoretical	Experimental	% Error
1 μg	2.0036	2.0463	2.13
10 μg		2.0515	2.39

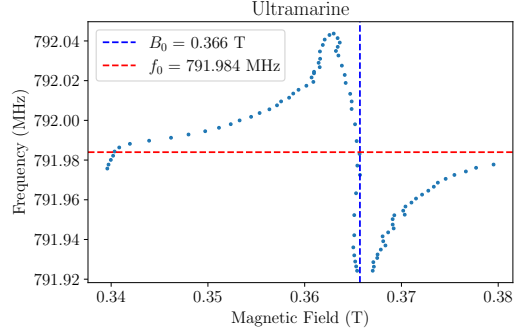
Table 1: Comparison between the theoretical and experimental g-factors of the DPPH samples.

The percent error for the 10 μg sample is slightly higher than that of the 1 μg sample. Theoretically, the values should be the same (as the material is unchanged), but a potential reason that the error increases is because at higher concentrations, more dipole interactions can occur which can shift the resonance condition slightly. This is also seen in the resonance frequency increasing from 792.451 MHz to 791.902 MHz in 13a and 13c respectively.

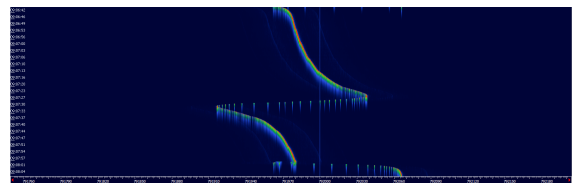
Other sources of error include the calibration of the axes and point assignment in the software.

2.4 Task 5: Determination of the resonance frequency and recording of the dispersion curves of different Ultramarine samples

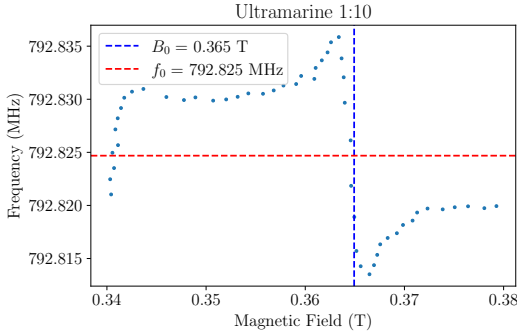
The same is done here as in the previous task, but with four Ultramarine samples of decreasing concentrations.



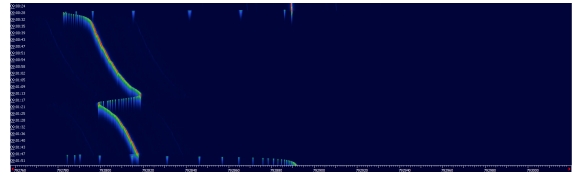
(a) Digitized dispersion curve of the undiluted Ultramarine sample. $B_0 = 0.366$ T, $f_0 = 791.984$ MHz.



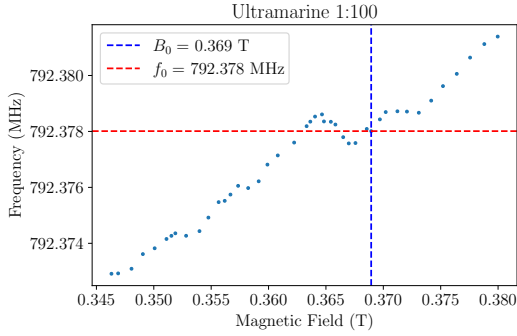
(b) Dispersion curve of the undiluted Ultramarine sample, as seen in HDSDR.



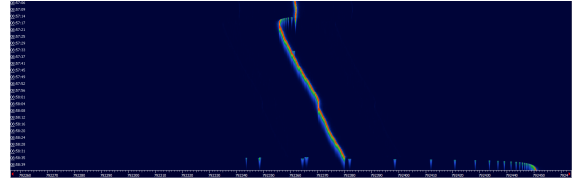
(c) Digitized dispersion curve of the 1:10 diluted Ultramarine sample. $B_0 = 0.365$ T, $f_0 = 792.825$ MHz.



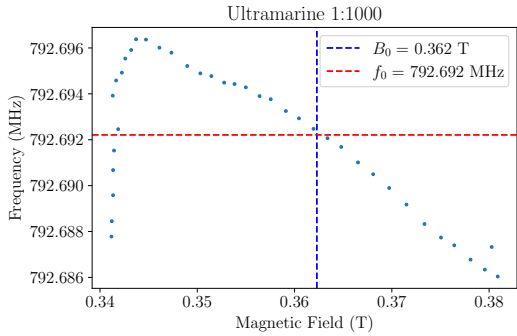
(d) Dispersion curve of the 1:10 diluted Ultramarine sample, as seen in HDSDR.



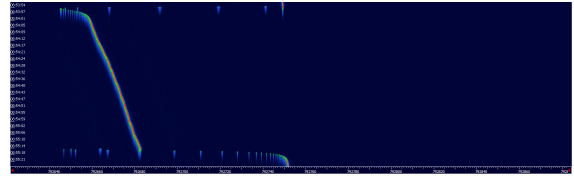
(e) Digitized dispersion curve of the 1:100 diluted Ultramarine sample. $B_0 = 0.369$ T, $f_0 = 792.378$ MHz.



(f) Dispersion curve of the 1:100 diluted Ultramarine sample, as seen in HDSDR.



(g) Digitized dispersion curve of the 1:1000 diluted Ultramarine sample. $B_0 = 0.362$ T, $f_0 = 792.692$ MHz.



(h) Dispersion curve of the 1:1000 diluted Ultramarine sample, as seen in HDSDR.

Figure 14

The following table shows the calculated g-factors for the four samples:

Ultramarine g-factor	Theoretical	Experimental	% Error
Undiluted	2.0290	2.0595	1.51
1:10		2.0641	1.73
1:100		2.0416	0.62
1:1000		2.0791	2.47

Table 2: Comparison between the theoretical and experimental g-factors of the Ultramarine samples.

The percent error for the 1:100 diluted sample is the lowest, while the 1:1000 diluted sample has the highest. Given the analysis of the previous task, one would expect the 1:1000 diluted sample to have the lowest error, but this is overshadowed by the fact that the resonance was impossible to detect at the lowest concentration, as it barely happened. Furthermore, the slight increase in percent error from undiluted to 1:10 can be attributed to software calibration issues.

Interestingly, Figure 14 shows that the resonance frequency increases, then decreases, then increases again (with the magnetic field behaving in the opposite manner) with increasing dilution. This is probably due to the fact that EPR can be a sensitive measurement, so any number of environmental factors could have affected the signal.

2.5 Task 6: Measurement of the DPPH sample 10 μ g with a calibrated LNB as observation system

Once again, this is very similar to task 4, but with a calibrated LNB such that the local oscillator has a frequency of exactly 9.75 GHz as the receiver.

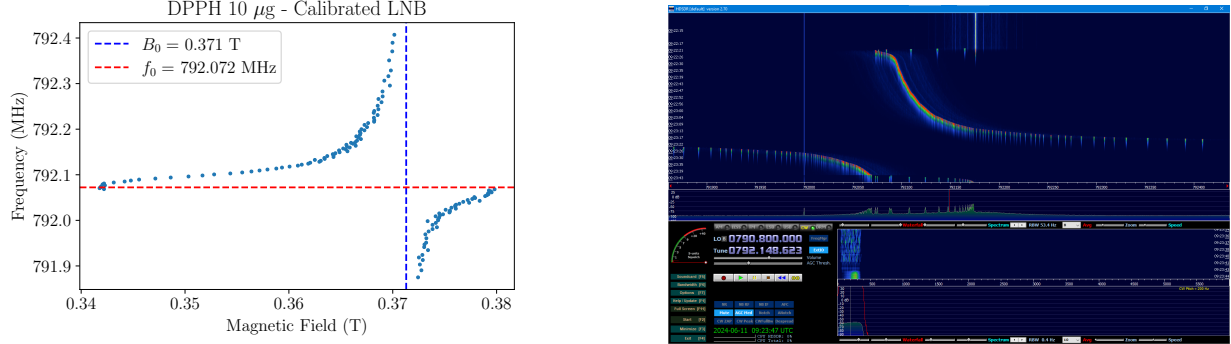


Figure 15

The g-factor for the 10 μ g DPPH sample is calculated to be 2.0286, close the theoretical value of 2.0036 (a 1.25% error).

Comparing the results for DPPH in this task and task 4, we obtain the following:

DPPH 10 μ g	Uncalibrated LNB	Calibrated LNB	Change from uncalibrated
g-factor	2.0515	2.0286	-1.12%
f_0	791.902	792.072	+0.17 MHz
B_0	0.367	0.371	+4 mT

Table 3: Comparison between the results of the 10 μ g DPPH sample with an uncalibrated and calibrated LNB.

Both resonance frequency and magnetic field increased slightly. In other tasks, when one increased the other would decrease. This is due to the fact that the LNB was calibrated to a different frequency, so the resonance condition was met at a different point.

The g-factor decreased slightly, and is more accurate now. This makes sense as the LNB was calibrated so the displayed magnetic field strength should be more accurate to the real value.

3 Conclusion

In *Task 1*, we observed the outputs from a frequency mixer with $f_1 = 10$ MHz and f_2 varying from 200 to 1000 kHz. The oscilloscope and HDSDR software outputs confirmed the expected frequency components, with the sum and difference frequencies $f_1 + f_2$ and $f_1 - f_2$ clearly visible. The presence of additional lines suggests possible interference or noise.

Task 2 involved receiving and analyzing signals in the VLF range from 10 kHz to 150 kHz using a simple radio transmitter. The frequency shifts observed when changing channels on the walkie-talkie confirmed the expected behavior of decreasing frequency increments.

Task 4 focused on determining the resonance frequency and recording dispersion curves for DPPH samples of different weights (1 μ g and 10 μ g). The g-factors calculated for the samples showed a small percent error from the theoretical value, with a slight increase in error for the higher concentration sample. Potential sources of error include dipole interactions at higher concentrations and calibration inaccuracies.

Task 5 repeated the process with four Ultramarine samples of decreasing concentrations. The g-factors showed varying percent errors, with the 1:100 diluted sample having the lowest error. The unexpected behavior of the resonance frequency and magnetic field with increasing dilution suggests environmental factors may have influenced the EPR measurements.

Task 6 measured the 10 μ g DPPH sample using a calibrated LNB, resulting in a g-factor of 2.0286. Comparing the results with the uncalibrated LNB showed a slight decrease in the g-factor and small increases in the resonance frequency and magnetic field strength. The calibration of the LNB improved the accuracy of the measurements.

Bibliography

- [1] automeris.io: Ai assisted data extraction from charts using webplotdigitizer. URL: <https://automeris.io/>.
- [2] Understand rf mixing & frequency mixers » electronics notes. URL: <https://www.electronics-notes.com/articles/radio/rf-mixer/rf-mixing-basics.php>.
- [3] Waveform for frequency modulation. URL: <https://electronicscoach.com/frequency-modulation.html/waveform-for-frequency-modulation>.
- [4] Electron paramagnetic resonance (epr) — zurich instruments, 12 2019. URL: <https://www.zhinst.com/europe/en/applications/nanotechnology-materials-science/electron-paramagnetic-resonance-epr>.
- [5] Dpph, 06 2020. URL: <https://en.wikipedia.org/wiki/DPPH>.
- [6] Wikipedia Contributors. Electron paramagnetic resonance, 08 2019. URL: https://en.wikipedia.org/wiki/Electron_paramagnetic_resonance.
- [7] Department of Physics and Geosciences. "electron-paramagnetic resonance (epr)", 2001. URL: https://home.uni-leipzig.de/physfp/manuals/EPR_englisch_11_2013.pdf.
- [8] Physics Department UIUC. Electron paramagnetic resonance, 1999. URL: https://home.uni-leipzig.de/physfp/manuals/EPR_englisch_11_2013.pdf.